Atmos. Chem. Phys. Discuss., 14, 7889–7916, 2014
www.atmos-chem-phys-discuss.net/14/7889/2014/
doi:10.5194/acpd-14-7889-2014

Atmospheric Chemistry and Physics Discussions
Open Access

The use of SMILES data to study ozone loss in the Arctic winter 2009/2010 and comparison with Odin/SMR data using assimilation techniques

K. Sagi[1], D. Murtagh[1], J. Urban[1], H. Sagawa[2], and Y. Kasai[2]

[1]Department of Earth and Space Sciences, Chalmers University of Technology, Gothenburg, Sweden
[2]National Institute of Information and Communications Technology, Tokyo, Japan

Received: 22 January 2014 – Accepted: 28 February 2014 – Published: 24 March 2014

Correspondence to: K. Sagi (sagi@chalmers.se)

Published by Copernicus Publications on behalf of the European Geosciences Union.

Abstract

The Superconducting Submillimeter-Wave Limb-Emission Sounder (SMILES) on board the International Space Station observed ozone profiles in the stratosphere with high sensitivity. Although SMILES measurements do not cover high latitudes, the combination of data assimilation methods and an isentropic advection model allows us to use SMILES measurements to investigate the ozone loss due to the instability of the polar vortex in the northern hemisphere. We quantified the ozone depletion in the 2009/2010 Arctic polar winter. Ozone data from both SMILES and Odin/SMR (Sub-Millimetre Radiometer) for the winter were assimilated into the Dynamical Isentropic Assimilation Model for OdiN Data (DIAMOND). DIAMOND is an off-line wind-driven transport model on isentropic surfaces. Wind data from the European Centre for Medium-Range Weather Forecasts (ECMWF) were used to drive the model. In this study, particular attention is paid to the cross isentropic transport of the tracer. The assimilated SMILES ozone fields agree with the SMR fields despite the limited latitude coverage. Ozone depletion has been derived by comparing the ozone field acquired by sequential assimilation with a passively transported ozone field initiated to 1 December 2009. Significant ozone loss was found in different periods and altitudes from using both SMILES and SMR data. The initial depletion occurred in the end of January below 500 K with a loss of 0.6–1.0 ppm (approximately 20 %). The ensuing loss started from the end of February between 575 K and 650 K. Our estimation shows that 0.8 ppmv (15–20 %) of O_3 has been removed from the lower stratosphere by 1 April in VMR.

1 Introduction

According to many studies of stratospheric ozone (O_3) over the Antarctic, O_3 depletion inside the isolated polar vortex is caused by the formation of Polar Stratospheric Clouds (PSC) and the associated heterogeneous release of active species such as chlorine (eg. Solomon, 1999). However, in comparison with the Antarctic polar vortex,

ACPD
14, 7889–7916, 2014

the Arctic vortex is unstable due to the propagation of planetary waves from the troposphere. Therefore the periods during which the temperature inside vortex goes below the threshold for PSC formation are highly irregular (WMO, 2011). This fact makes the quantification of chemical O_3 depletion in the Arctic generally more difficult.

The winter of 2009–2010 was one of the colder winters in the last decade. Figure 1 indicates the minimum temperature (T_{min}) derived from the European Centre for Medium-Range Weather Forecasts (ECMWF) operations on the 600 K potential temperature (PT) surface at equivalent latitudes (EQL) greater than 70° N. The T_{min} for the winter period of 2009–2010 decreased until 7 January and reached as low as 180 K. Khosrawi et al. (2011) reported that strong denitrification caused by the formation of the PSCs was observed during the synoptic cooling event in mid-January 2010. However, a Sudden Stratospheric Warming (SSW) ended the coldest period after 19 January. SSWs are wintertime phenomena that are characterized by suddenly increasing temperatures and a reversal of the zonal wind (Scherhag, 1952). In addition to the instability of the vortex, the occurrence of the SSW event makes this winter dynamically complicated.

SMILES (Superconducting subMIllimeter-wave Limb Emission Sounder), a passive atmospheric sensor attached to the Japanese Experiment Module (JEM) on board the International Space Station (ISS), was developed by the Japan Aerospace Exploration Agency (JAXA) and the National Institute of Information and Communications Technology (NICT). SMILES used a 4 K superconducting detector technology to measure high precision vertical profiles of stratospheric and mesospheric species related to ozone chemistry. The instrument was operated from October 2009 until April 2010 providing atmospheric composition data typically within the latitude range of 38–65° S (Kikuchi et al., 2010).

The subject of this paper is to demonstrate the use of the high sensitivity observations by SMILES to quantify polar ozone loss. However, it is still a challenge to use SMILES data to analyze the polar regions because of its latitude coverage. Figure 2a shows a typical observation map of SMILES (and Odin/SMR). Neverthless, the dynamical instability of this winter season permitted a considerable number of SMILES observations within the vortex. The number of O_3 measurements for both SMILES and Odin/SMR inside the vortex (EQL $\geq$ 70) per day are plotted in Fig. 2b. The higher vertical scan rate of SMILES compared to SMR explains the larger number of measurements. On the other hand, there are periods when SMILES measurements inside the vortex were missing. In the first half of December, the field of view of the SMILES antenna was blocked by the ISS solar paddles at high latitudes, resulting in few useable measurements. An other empty period, in the middle of February, is due to the rotation of the ISS to dock with the space shuttle Endeavour. When the space shuttle was docked, the ISS was rotated by 180° and SMILES looked towards the Southern Hemisphere.

In this paper, we employed the data assimilation technique developed for other Arctic winters by Rösevall et al. (2007a, b, 2008) to investigate the O_3 depletion in the 2009/2010 winter using SMILES O_3 data. Other authors have used various models and assimilation methods in similar studies (El Amraoui et al., 2008; Jackson and Orsolini, 2008; Søvde et al., 2011). One advantage of data assimilation is that it allows us to optimally use all measurements and is useful for interpolating or extrapolating the O_3 distributions when and where no measurements are available. In this study we have also used the DIAMOND assimilation model developed by Rösevall et al. (2007b). However, because the model works in two dimensions, Rösevall et al. (2007a, b, 2008) needed to account for the effect of the diabatic descent inside the vortex a posteriori. Thus we have implemented a new vertical transport scheme that continuously accounts for the decent rather than an a-posteriori correction. O_3 observed by SMR is also analyzed for comparison. This paper is structured as follows. Sections 2 and 3 describe the measurement and model, respectively. Section 4 tests the effectiveness of the new vertical transport scheme using the long lived species N_2O measured by SMR and then shows the results of the O_3 analyses. Finally, we conclude the study in Sect. 5.

ACPD
14, 7889–7916, 2014

2 Measurement descriptions

Profiles of O_3 were obtained from the SMILES and SMR instruments. Nitrous oxide (N_2O) from SMR was also used for this study. N_2O is generally used as a tracer of transport in the stratosphere due to its long lifetime.

2.1 SMILES

SMILES observed atmospheric limb emission from the ISS at an altitude of 340–360 km. It vertically scans the tangent heights of ~ -20–120 km with an antenna field-of-view of ~ 3 km. A single spectrum is obtained with a data integration time of 0.47 s, and one vertical scan takes 53 s including the calibration data acquisition. About 1630 scans are obtained per day. Because the ISS has a non sun-synchronous orbit, the local time of SMILES measurement location evolves over 24 h after 1–2 month.

SMILES detects the submillimeter emission of O_3 at 625.371 GHz. The spectra are spectrally resolved with an Acousto-Optical Spectrometer (AOS) which has a bandwidth of 1.2 GHz and a resolution of 1.2 MHz. There are three instrumental configurations for the SMILES O_3 625.371 GHz observations: two different observation frequency bands (named band-A and B hereafter) and two different AOS units. The measurement noise of SMILES is as low as < 0.7 K (for a single AOS channel and a single spectrum) due to the low noise performance of the superconductor-insulator-superconductor (SIS) mixers. See Kikuchi et al. (2010) and Kasai et al. (2013) for further detail about the SMILES instrumentation.

We used the O_3 data produced by the NICT level-2 chain version 2.1.5. This level-2 chain employs the least-squares method with a priori regularization (e.g. Rodgers, 2000) as described by Baron et al. (2011). The O_3 profile is retrieved from 16 to 90 km with a vertical resolution of ~ 3–4 km and ~ 6–10 km for the stratosphere and mesosphere, respectively. The validation of this version of SMILES NICT O_3 data is described by Kasai et al. (2013). Based on the error analysis and comparison studies of mid-latitude O_3 data, they reported the systematic error is better than 0.3 ppmv in the

ACPD
14, 7889–7916, 2014

stratosphere (~ 60–8 hPa). The random error for a single O_3 profile is as low as 1 % for this altitude region. It is also reported that the data quality of O_3 profile from band-B is better than that from band-A.

2.2 Odin/SMR

Odin is a Swedish satellite mission in association with Canada, Finland and France, which was designed for radio astronomy and limb sounding of the Earth's middle atmosphere (Murtagh et al., 2002). Odin was launched on 20 February 2001 into a sun-synchronous polar orbit with an inclination of 98°, altitude of ~ 600 km and descending and ascending nodes at 6 and 18 h LST respectivly. It carries two different limb sounding instruments, OSIRIS (Optical Spectro- graph/InfraRed Imaging System) and SMR (Sub-Millimetre Radiometer). The SMR instrument, described by (Frisk et al., 2003), consists of four tunable single-sideband Schottky-diode heterodyne microwave receivers.

The datasets for O_3 and N_2O from SMR used in this paper are products of the stratospheric mode that is operated every other day since April 2007 (every third day previous to this). In the stratospheric observation mode, two of the receivers, covering the bands centered at 501.8 and 544.6 GHz, are used for detecting the spectral emission lines of O_3, N_2O, ClO and HNO_3. The O_3 and N_2O profiles are retrieved from emission lines 501.5 GHz and 502.3 GHz, respectively, using the Chalmers version 2.1 retrieval scheme.

The SMR O_3 profiles cover the altitude range ~ 17–50 km with an altitude resolution of 2.5–3.5 km and an estimated single-profile precision of ~ 1.5 ppmv (Urban et al., 2005a). SMR v2.1 O_3 data has been validated against balloon sonde measurements as described in detail by (Jones et al., 2007). It shows that SMR O_3 in the 60–90° S latitude band has mixing ratios that are 0.0–0.1 ppmv lower than sonde measurements below 23 km and a positive bias of 0.1–0.3 ppmv in the 23 to 30 km range. The validation study (Kasai et al., 2013) shows that SMILES generally gives slightly lower O_3 values than SMR at altitudes below 20 hPa.

ACPD
14, 7889–7916, 2014

The N_2O profiles cover altitudes in the range 12–60 km with an altitude resolution of ∼ 1.5 km. The estimated systematic error is less than 12 ppbv (Urban et al., 2005a). The validation of the N_2O is reported by Urban et al. (2005b). Other measurement comparisons with the Fourier Transform Spectrometer (FTS) onboard the Atmospheric Chemistry Experiment (ACE) and the Microwave Limb Sounder (MLS) on the Earth Observing System (EOS) Aura satellite are shown by Strong et al. (2008) and Lambert et al. (2007), respectively.

3 DIAMOND model

The DIAMOND (Dynamic Isentropic Assimilation Model for OdiN Data) model is an off-line wind driven isentropic transport and assimilation model designed to simulate quasi-horizontal ozone transport in the lower stratosphere with low numerical diffusion. Isentropic off-line wind driven advection has been implemented using the Prather transport scheme (Prather, 1986) which is a mass conservative Eulerian scheme. The idea of the Prather scheme is that by preserving the zero to second order moments of the sub-grid scale tracer distribution the quality of the transport is preserved. In this study, the wind fields from the operational analyses of the ECMWF have been used. Advection calculations are performed on separate layers with a constant potential temperature (PT) range from 400 K to 1000 K in 25 K intervals.

The tracer profiles from SMILES or SMR are sequentially assimilated into the advection model. The assimilation scheme in DIAMOND is described as a variant of the Kalman filter. Details on the assimilation scheme can be found in Rösevall et al. (2007b).

3.1 Cross-isentropic transport

Under adiabatic conditions, PT is conservative in dry air and thus the air parcels normally move on a constant PT surface. However, during the polar night the condition

ACPD
14, 7889–7916, 2014

for adiabatic transport often breaks down due to strong radiative cooling of air masses inside the polar vortex. Thus, quantification of adiabatic vortex descent is necessary to correctly evaluate the ozone loss.

To account for this we implemented a simple vertical transport scheme into DIAMOND. This scheme is based on the one dimensional first-order upstream method, the equations for which are given below (1, 2). For the tracer distribution function $\Psi(\Theta, t)$ at a given vertical coordinate in potential temperature and time, Θ and t, we get

$$\frac{\partial \Psi}{\partial t} + \varpi \frac{\partial \Psi}{\partial \Theta} = 0 \tag{1}$$

$$\Psi(\Theta, t + \Delta t) = \Psi(\Theta, t)\left(1 - \varpi \frac{\mathrm{d}t}{\mathrm{d}\Theta}\right) + \Psi(\Theta - \Delta\Theta, t)\,\varpi \frac{\mathrm{d}t}{\mathrm{d}\Theta} \tag{2}$$

Here, ϖ is the vertical component of air mass advection. The first-order upstream method often produces numerical diffusion. In order to avoid this, it is necessary to satisfy the following condition,

$$\frac{\Delta\Theta}{\Delta t} > C \tag{3}$$

Here $\Delta\Theta$, Δt and C represent the grid interval, the time step and the speed of the phenomenon, respectively. The $\Delta\Theta/\Delta t$ in the model ($= 2.5\,\mathrm{K\,min^{-1}}$) is much larger than the general descent rate inside the polar vortex ($\sim 1\,\mathrm{K\,day^{-1}}$), and therefore the first-order upstream method can be used satisfactorily.

To quantify the vertical transport, we used the diabatic heating rate Q [$\mathrm{K\,s^{-1}}$] derived from SLIMCAT 3d chemical transport model calculations (Chipperfield, 2006). The vertical velocity ϖ was calculated as,

$$\varpi = \left(\frac{\Theta}{T}\right) \cdot Q \tag{4}$$

where, Θ and T are potential and absolute temperatures, respectively.

ACPD
14, 7889–7916, 2014

4 Results

4.1 Dynamics of the Arctic winter 2009–2010

In order to test the performance of the model and study the dynamics of this winter, we modelled stratospheric N_2O fields by assimilation of SMR N_2O. A summary of the calculations is given in Table 1. Initialization (i.e. the spin up calculations with assimilations) for one month prior to the investigation period is required to ensure the accuracy of the initial model field. In order to remove contamination by the erroneous observations, the SMR data is used only if the measurement response is larger than 0.85. To reduce any boundary condition problems realistic tracer fields are required. Boundary layers at PT of 400 K and 1000 K have also been produced by the assimilation for the analysis period in advance. These are used as buffer layers to feed the vertical transport scheme. Note that the measurement response especially for SMR N_2O is generally less than 0.7 at lower altitudes (< 450 K). So that we relaxed the measurement response threshold to 0.7 for the boundaries. In the results, we only show the output of the model from 425 K to 950 K. The uncertainty of the DIAMOND model due to imperfections in the transport scheme and/or unimplemented chemical processes has to be considered. We set the initial error fields to 30 % of the US standard atmosphere, which corresponds to the standard variation of the 40 days prediction without assimilations. The error field grows linearly to this value in 40 days if no measurements are available.

Figure 3 shows the model results for N_2O and the corresponding error fields at 600 K. The polar vortex is clearly seen as the area where the volume mixing ratio of N_2O is low. The polar vortex was formed at the beginning of winter and stayed at high latitudes for one to two weeks then distorted and divided in two parts caused by changes in the wind fields due to a minor SSW in the middle of December. The two separate vortices had reconnected by 17 December. After that, the vortex stayed cold and remained pole centered until the major SSW occurred at the end of January 2010 (eg. Dörnbrack et al., 2012). This period contained the coldest temperatures of this winter (see Fig. 1).

ACPD
14, 7889–7916, 2014

The major SSW changed the wind field again: massive inflow of air from the Pacific forced the vortex to move to middle latitudes with flattening over Eurasia. Furthermore, the vortex again split after 10 February. Finally, when the polar night ended, the vortex broke and the vortex air horizontally mixed with air from outside.

To illustrate the advection in the DIAMOND model, we derived the vortex mean of N_2O from the daily fields. Figure 4 shows the mean of the N_2O concentrations inside the area where the EQL is greater equal than 70°. The solid lines in the figure are calculated from results of assimilation of SMR N_2O. The two dashed lines, black and gray, are the vortex mean of the fields predicted by the advection model using the initial N_2O distribution as of 1 December with and without vertical transport, respectively. If the vertical transport is perfectly simulated in the model, the black predicted N_2O line should match the one with assimilated data. Compared to the predictions from the 2-D advection, the ones with the vertical transport scheme shows good agreement with the vortex mean assimilated N_2O field until the final break up of the vortex. The uncertainty of the mean, plotted as the shaded areas in Fig. 4, is calculated as $\sqrt{\sigma^2 + \hat{E}^2}$. Here σ and $\hat{E}$ are the standard deviation of N_2O inside the vortex and the vortex mean of the error field, respectively. More details of these components can be seen in Fig. 5. $\hat{E}$ characterizes the error from the point of view of the instrument. However the dominant factor in the uncertainties is the variability inside the vortex (σ). The temporal evolution of σ allows us to assess the contribution of the (mostly horizontal) mixing. At the end of February (approximately 50 days from 1 January), there are exponential increases in σ caused by the breaking of the vortex and associated mixing. This is particularly noticeable above 550 K.

4.2 O_3 inside the vortex

Figure 6 displays maps of the results for O_3 from the assimilations of data from SMR and SMILES.

ACPD
14, 7889–7916, 2014

The results from the two instruments have similar patterns in the O_3 maps although those from the SMR exhibit more features and larger variations. The reasons for the differences are the number and quality of measurements. Specifically, SMR has fewer measurements at lower latitudes because of its orbit and has a higher noise level. The SMILES O_3 abundance, as expected due to known biases, was slightly lower than SMR O_3 below 700 K corresponding to 20 hPa in pressure (see Fig. 20 in Kasai et al., 2013). An other important point is the incomplete coverage of the center of the vortex for the SMILES assimilation. As noted in the introduction, SMILES did not observe at higher latitudes than 65° S. As a result the information on O_3 in the polar region is transported from lower latitudes by the model. Thus, when the vortex is stable and well isolated, modeled O_3 distributions may deviate from the true atmosphere. This is clearly seen in the SMILES O_3 maps at the end of December where higher concentrations compared to earlier are seen inside the vortex due to the descent from higher levels and the lack of any chemical O_3 loss processes in the model.

To avoid the effects of large local variations, we have chosen to use the average for the entire vortex for this study. The sampling issues described above are mitigated by employing a weighted average over the vortex as shown in the Fig. 7. The weights are given by estimated model error fields. Note the fact that the vortex mean of the SMILES assimilation thereby emphasizes the contribution near the vortex edge. Vortex averages of O_3 from both instruments show similar patterns, especially before the major SSW event at the end of January. Uncertainties in Fig. 7 are also calculated using the standard deviation σ and the mean of the error field $\hat{E}$ inside the vortex. Since SMR O_3 is much noisier, information on the mixing from the vortex internal variation of O_3 fields σ are masked by the average error fields $\hat{E}$, while for SMILES the total error reflects the variation inside the vortex.

Arctic O_3 depletion is estimated by subtracting O_3 fields passively transported in the DIAMOND model from the fields with assimilated data. The time evolution of the O_3 losses derived from SMILES and SMR are presented in Fig. 8a and b. O_3 losses inferred from the two instruments have similar patterns. The first significant depletion

ACPD
14, 7889–7916, 2014

occurred below 500 K from 25 January to 7 February: this corresponds to the period when the vortex moved towards lower latitudes and becomes exposed to sunlight. The loss rate is approximately 0.06 ppm day^{-1}. Within two weeks, catalytic O_3 depletion reached equilibrium with the photochemical production and the horizontal mixing due to unstable conditions after the SSW. The second loss took place from the end of February at the heights between 575 K and 650 K. This continued even after the vortex break up at a rate of 0.03 ~ 0.04 ppm day^{-1}. Figure 9 presents the monthly mean of the accumulated ozone loss for March 2010. The first and second losses occurred at different altitudes and are clearly seen in the profiles of O_3 loss as peaks around 500 K and 600 K, respectively. O_3 loss as estimated from SMILES is slightly larger at most levels. It is proposed that the difference in O_3 loss between the two instruments is a result of sampling issues. SMILES captures O_3 changes near the vortex edge where the area has been more exposed to sunlight while SMR on the other hand represents the loss at the centre of the vortex because of its orbit.

The initial loss from 25 January below 500 K can be explained using the classical mechanism related to heterogeneous reactions on PSCs and the chlorine catalytic cycle (Solomon, 1988). Generally, PSCs are classified according to the air temperature above (type I) and below (type II) the water ice frost point (T_{ice}). Type I PSCs mainly consist of particles of Nitric Acid Tri-hydrate (NAT). From mid December until the middle of January, the temperature inside the vortex was cold enough to form PSC not only for type I but also type II (Fig. 8f–h). Khosrawi et al. (2011) found that due to an unusually strong synoptic cooling event in mid January, ice particle formation on NAT may be a possible formation mechanism causing the denitrification observed in mid January. Vortex average ClO in daytime and nighttime are also presented in Fig. 8c and d. Here, ClO profiles have been retrieved from the frequency band centered at 501.8 GHz of SMR (Urban et al., 2005a). To group ClO into day and night time, we used solar zenith angles (SZA) of 90° and 95° as limits to avoid the twilight. The enhancement of ClO appears at 29 January at 475 K in advance of the O_3 depletion and confirms the

ACPD
14, 7889–7916, 2014

hypothesis that chlorine has been activated through heterogeneous chemistry involving PSCs.

However, it is difficult to explain the upper-level (575 K to 650 K) ozone loss from the end of February by only chlorine-related destruction. The second loss is correlated with the sun exposure time inside the vortex (shown in Fig. 8e). Nevertheless, the vortex average ClO is still low at around 600 K (Fig. 8c). Similar losses were also found in other winters (Konopka et al., 2007; Grooß and Müller, 2007; Jackson and Orsolini, 2008; Søvde et al., 2011). Konopka et al. (2007) discussed that the loss around 650 K in 2002/2003 was induced by the catalytic cycles of NO_x transported from the mesosphere and lower latitudes.

5 Conclusions

Datasets from SMILES and SMR have been used to quantify O_3 loss inside the polar vortex for the Arctic winter 2009–2010. The investigation was performed using the DIAMOND data assimilation framework. DIAMOND is an off-line wind-driven transport model advecting air on isentropic surfaces into which we introduced the vertical/cross-isentropic transport. Assimilation of SMR N_2O was used to verify the cross-isentropic scheme when using SLIMCAT heating rates to calculate the diabatic descent.

We have demonstrated that indeed SMILES measurements with data assimilation technique can be used to study ozone loss at high latitudes. O_3 fields from assimilation of SMILES and SMR showed similar patterns, although the quality and coverage of measurements caused differences between the O_3 fields, especially at lower latitudes. The agreement is also seen in the time evolutions of weighted vortex mean of O_3.

Ozone loss was derived by comparing fields acquired by sequential assimilation with passively transported fields. Significant losses are seen at different altitudes using both SMILES and SMR data and can be explained as follows: (I) Before the major SSW (~ 21 January), the reasonably stable and isolated polar vortex remained centered around the north pole and cold temperature allowed the formation of PSCs. (II) The

ACPD
14, 7889–7916, 2014

SSW changed the wind field and the inflow of air from the Pacific pushed the vortex out towards middle latitudes. (III) The first rapid O_3 depletion occurred below 500 K mostly close to the vortex edge where the polar night had ended (from 21 January to 7 February). The depletion is considered to be a result of ClO catalytic destruction. (IV) From 7 February, the second loss in the height range 575 K to 650 K started and continued until vortex break up. This loss might be induced by the NO_x reactions as discussed by Konopka et al. (2007). Further study is required to fully understand the mechanisms.

The monthly mean O_3 loss for March derived from SMILES was higher than that from SMR by 0–5 % and it can be attributed to loss occurring near the vortex edge. The initial peak of O_3 loss at lower levels was 0.7 ppmv (15–20 %) at 475 K for SMR O_3 and 1 ppmv (20–25 %) at 500 K for SMILES O_3, respectively. The second loss at 600 K was 0.8 ppmv (15–20 %) for both instruments.

Acknowledgements. We thank Martyn Chipperfield and Wuhu Feng in University of Leeds for providing the diabatic heating rate for this study and the Swedish National Space Board (SNSB) for funding.

References

Baron, P., Urban, J., Sagawa, H., Möller, J., Murtagh, D. P., Mendrok, J., Dupuy, E., Sato, T. O., Ochiai, S., Suzuki, K., Manabe, T., Nishibori, T., Kikuchi, K., Sato, R., Takayanagi, M., Murayama, Y., Shiotani, M., and Kasai, Y.: The Level 2 research product algorithms for the Superconducting Submillimeter-Wave Limb-Emission Sounder (SMILES), Atmos. Meas. Tech., 4, 2105–2124, doi:10.5194/amt-4-2105-2011, 2011. 7893

Chipperfield, M. P.: New version of the TOMCAT/SLIMCAT off-line chemical transport model: intercomparison of stratospheric tracer experiments, Q. J. Roy. Meteor. Soc., 132, 1179–1203, doi:10.1256/qj.05.51, 2006. 7896

Dörnbrack, A., Pitts, M. C., Poole, L. R., Orsolini, Y. J., Nishii, K., and Nakamura, H.: The 2009–2010 Arctic stratospheric winter – general evolution, mountain waves and predictability of an operational weather forecast model, Atmos. Chem. Phys., 12, 3659–3675, doi:10.5194/acp-12-3659-2012, 2012. 7897

El Amraoui, L., Semane, N., Peuch, V. H., and Santee, M. L.: Investigation of dynamical processes in the polar stratospheric vortex during the unusually cold winter 2004/2005, Geophys. Res. Lett., 35, L03803, doi:10.1029/2007GL031251, 2008. 7892

Frisk, U., Hagström, M., Ala-Laurinaho, J., Andersson, S., Berges, J. C., Chabaud, J. P., Dahlgren, M., Emrich, A., Florén, H. G., Florin, G., Fredrixon, M., Gaier, T., Haas, R., Hirvonen, T., Hjalmarsson, Å., Jakobsson, B., Jukkala, P., Kildal, P. S., Kollberg, E., Lassing, J., Lecacheux, A., Lehikoinen, P., Lehto, A., Mallat, J., Marty, C., Michet, D., Narbonne, J., Nexon, M., Olberg, M., Olofsson, A. O. H., Olofsson, G., Origné, A., Petersson, M., Piironen, P., Pons, R., Pouliquen, D., Ristorcelli, I., Rosolen, C., Rouaix, G., Räisänen, A. V., Serra, G., Sjöberg, F., Stenmark, L., Torchinsky, S., Tuovinen, J., Ullberg, C., Vinterhav, E., Wadefalk, N., Zirath, H., Zimmermann, P., and Zimmermann, R.: The Odin satellite, Astron. Astrophys., 402, L27–L34, doi:10.1051/0004-6361:20030335, 2003. 7894

Grooß, J. U. and Müller, R.: Simulation of ozone loss in Arctic winter 2004/2005, Geophys. Res. Lett., 34, L05804, doi:10.1029/2006GL028901, 2007. 7901

Jackson, D. R. and Orsolini, Y. J.: Estimation of Arctic ozone loss in winter 2004/05 based on assimilation of EOS MLS and SBUV/2 observations, Q. J. Roy. Meteor. Soc., 134, 1833–1841, doi:10.1002/qj.316, 2008. 7892, 7901

Jones, A., Murtagh, D., Urban, J., Eriksson, P., and Rosevall, J.: Intercomparison of Odin/SMR ozone measurements with MIPAS and balloonsonde data, Can. J. Phys., 85, 1111–1123, 2007. 7894

Kasai, Y., Sagawa, H., Kreyling, D., Dupuy, E., Baron, P., Mendrok, J., Suzuki, K., Sato, T. O., Nishibori, T., Mizobuchi, S., Kikuchi, K., Manabe, T., Ozeki, H., Sugita, T., Fujiwara, M., Irimajiri, Y., Walker, K. A., Bernath, P. F., Boone, C., Stiller, G., von Clarmann, T., Orphal, J., Urban, J., Murtagh, D., Llewellyn, E. J., Degenstein, D., Bourassa, A. E., Lloyd, N. D., Froidevaux, L., Birk, M., Wagner, G., Schreier, F., Xu, J., Vogt, P., Trautmann, T., and Yasui, M.: Validation of stratospheric and mesospheric ozone observed by SMILES from International Space Station, Atmos. Meas. Tech., 6, 2311–2338, doi:10.5194/amt-6-2311-2013, 2013. 7893, 7894, 7899

Khosrawi, F., Urban, J., Pitts, M. C., Voelger, P., Achtert, P., Kaphlanov, M., Santee, M. L., Manney, G. L., Murtagh, D., and Fricke, K.-H.: Denitrification and polar stratospheric

ACPD
14, 7889–7916, 2014

cloud formation during the Arctic winter 2009/2010, Atmos. Chem. Phys., 11, 8471–8487, doi:10.5194/acp-11-8471-2011, 2011. 7891, 7900

Kikuchi, K.-i., Nishibori, T., Ochiai, S., Ozeki, H., Irimajiri, Y., Kasai, Y., Koike, M., Manabe, T., Mizukoshi, K., Murayama, Y., Nagahama, T., Sano, T., Sato, R., Seta, M., Takahashi, C., Takayanagi, M., Masuko, H., Inatani, J., Suzuki, M., and Shiotani, M.: Overview and early results of the Superconducting Submillimeter-Wave Limb-Emission Sounder (SMILES), J. Geophys. Res., 115, D23306, doi:10.1029/2010JD014379, 2010. 7891, 7893

Konopka, P., Engel, A., Funke, B., Müller, R., Grooß, J.-U., Günther, G., Wetter, T., Stiller, G., von Clarmann, T., Glatthor, N., Oelhaf, H., Wetzel, G., López-Puertas, M., Pirre, M., Huret, N., and Riese, M.: Ozone loss driven by nitrogen oxides and triggered by stratospheric warmings can outweigh the effect of halogens, J. Geophys. Res., 112, D05105, doi:10.1029/2006JD007064, 2007. 7901, 7902

Lambert, A., Read, W. G., Livesey, N. J., Santee, M. L., Manney, G. L., Froidevaux, L., Wu, D. L., Schwartz, M. J., Pumphrey, H. C., Jimenez, C., Nedoluha, G. E., Cofield, R. E., Cuddy, D. T., Daffer, W. H., Drouin, B. J., Fuller, R. A., Jarnot, R. F., Knosp, B. W., Pickett, H. M., Perun, V. S., Snyder, W. V., Stek, P. C., Thurstans, R. P., Wagner, P. A., Waters, J. W., Jucks, K. W., Toon, G. C., Stachnik, R. A., Bernath, P. F., Boone, C. D., Walker, K. A., Urban, J., Murtagh, D., Elkins, J. W., and Atlas, E.: Validation of the Aura Microwave Limb Sounder middle atmosphere water vapor and nitrous oxide measurements, J. Geophys. Res., 112, D24S36, doi:10.1029/2007JD008724, 2007. 7895

Murtagh, D., Frisk, U., Merino, F., Ridal, M., Jonsson, A., Stegman, J., Witt, G., Eriksson, P., Jiménez, C., Megie, G., Noë, J. D. L., Ricaud, P., Baron, P., Pardo, J. R., Hauchcorne, A., Llewellyn, E. J., Degenstein, D. A., Gattinger, R. L., Lloyd, N. D., Evans, W. F., McDade, I. C., Haley, C. S., Sioris, C., Savigny, C. V., Solheim, B. H., McConnell, J. C., Strong, K., Richardson, E. H., Leppelmeier, G. W., Kyrölä, E., Auvinen, H., and Oikarinen, L.: An overview of the Odin atmospheric mission, Can. J. Phys., 80, 309–319, 2002. 7894

Prather, M. J.: Numerical advection by conservation of second-order moments, J. Geophys. Res., 91, 6671–6681, doi:10.1029/JD091iD06p06671, 1986. 7895

Rodgers, C. D.: Inverse Methods for Atmospheric Sounding: Theory and Practice, Series on Atmospheric, Oceanic and Planetary Physics, Vol. 2, Singapore, World Scientific, 2000. 7893

Rösevall, J. D., Murtagh, D. P., and Urban, J.: Ozone depletion in the 2006/2007 Arctic winter, Geophys. Res. Lett., 34, L21809, doi:10.1029/2007GL030620, 2007a. 7892

Rösevall, J. D., Murtagh, D. P., Urban, J., and Jones, A. K.: A study of polar ozone depletion based on sequential assimilation of satellite data from the ENVISAT/MIPAS and Odin/SMR instruments, Atmos. Chem. Phys., 7, 899–911, doi:10.5194/acp-7-899-2007, 2007b. 7892, 7895

Rösevall, J. D., Murtagh, D. P., Urban, J., Feng, W., Eriksson, P., and Brohede, S.: A study of ozone depletion in the 2004/2005 Arctic winter based on data from Odin/SMR and Aura/MLS, J. Geophys. Res., 113, D13301, doi:10.1029/2007JD009560, 2008. 7892

Scherhag, R.: Die explosionsartige Stratosphärenerwärmung des Spätwinters 1951/52, Berichte des Deutschen Wetterdienstes, 38, 51–63, 1952. 7891

Solomon, S.: The mystery of the Antarctic "Ozone Hole", Rev. Geophys., 26, 131–148, doi:10.1029/RG026i001p00131, 1988. 7900

Solomon, S.: Stratospheric ozone depletion: a review of concepts and history, Rev. Geophys., 37, 275–316, doi:10.1029/1999RG900008, 1999. 7890

Søvde, O. A., Orsolini, Y. J., Jackson, D. R., Stordal, F., Isaksen, I. S. A., and Rognerud, B.: Estimation of Arctic O_3 loss during winter 2006/2007 using data assimilation and comparison with a chemical transport model, Q. J. Roy. Meteor. Soc., 137, 118–128, doi:10.1002/qj.740, 2011. 7892, 7901

Strong, K., Wolff, M. A., Kerzenmacher, T. E., Walker, K. A., Bernath, P. F., Blumenstock, T., Boone, C., Catoire, V., Coffey, M., De Mazière, M., Demoulin, P., Duchatelet, P., Dupuy, E., Hannigan, J., Höpfner, M., Glatthor, N., Griffith, D. W. T., Jin, J. J., Jones, N., Jucks, K., Kuellmann, H., Kuttippurath, J., Lambert, A., Mahieu, E., McConnell, J. C., Mellqvist, J., Mikuteit, S., Murtagh, D. P., Notholt, J., Piccolo, C., Raspollini, P., Ridolfi, M., Robert, C., Schneider, M., Schrems, O., Semeniuk, K., Senten, C., Stiller, G. P., Strandberg, A., Taylor, J., Tétard, C., Toohey, M., Urban, J., Warneke, T., and Wood, S.: Validation of ACE-FTS N_2O measurements, Atmos. Chem. Phys., 8, 4759–4786, doi:10.5194/acp-8-4759-2008, 2008. 7895

Urban, J., Lautié, N., Le Flochmoën, E., Jiménez, C., Eriksson, P., de La Noë, J., Dupuy, E., Ekström, M., El Amraoui, L., Frisk, U., Murtagh, D., Olberg, M., and Ricaud, P.: Odin/SMR limb observations of stratospheric trace gases: Level 2 processing of ClO, N_2O, HNO_3, and O_3, J. Geophys. Res, 110, D14307, doi:10.1029/2004JD005741 2005a. 7894, 7895, 7900

Urban, J., Lautié, N., Le Flochmoën, E., Jiménez, C., Eriksson, P., de La Noë, J., Dupuy, E., El Amraoui, L., Frisk, U., Jégou, F., Murtagh, D., Olberg, M., Ricaud, P., Camy-Peyret, C., Dufour, G., Payan, S., Huret, N., Pirre, M., Robinson, A. D., Harris, N. R. P., Bremer, H.,

ACPD
14, 7889–7916, 2014

Arctic ozone loss during 2009–2010 from Odin/SMR and SMILES

K. Sagi et al.

Kleinböhl, A., Küllmann, K., Künzi, K., Kuttippurath, J., Ejiri, M. K., Nakajima, H., Sasano, Y., Sugita, T., Yokota, T., Piccolo, C., Raspollini, P., and Ridolfi, M.: Odin/SMR limb observations of stratospheric trace gases: validation of N_2O, J. Geophys. Res., 110, D09301, doi:10.1029/2004JD005394, 2005b. 7895

WMO: Scientific Assessment of Ozone Depletion: 2010, Global Ozone Research and Monitoring Project-Report No. 52, 516 pp., Geneva, Switzerland, 2011. 7891

ACPD

14, 7889–7916, 2014

Arctic ozone loss during 2009–2010 from Odin/SMR and SMILES

K. Sagi et al.

Table 1. Description of the calculations.

Condition	Value
Time period	1 Dec 2009 ~ 31 Mar 2010
Initialisation	1 month (1 Nov 2009 ~ 1 Dec 2009)
Altitude range (EPT)	425 K ~ 950K (25 K resolution)
Measurement Response	≥ 0.85

ACPD
14, 7889–7916, 2014

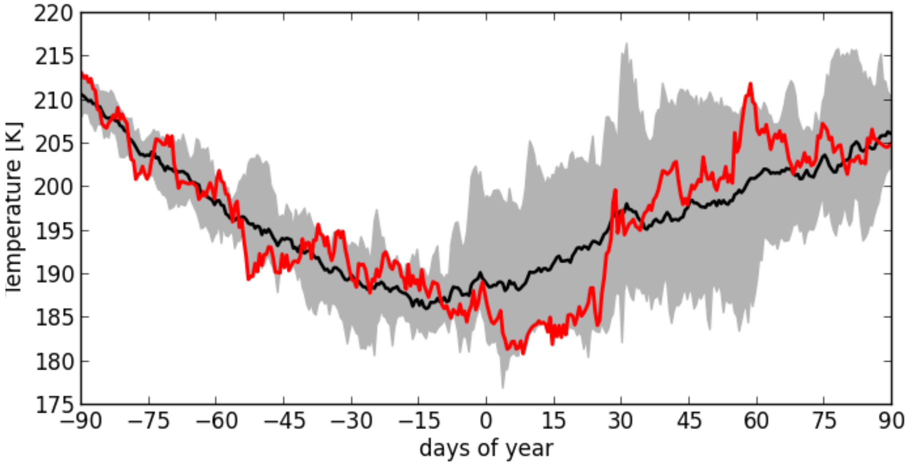

Fig. 1. Minimum ECMWF temperature, T_{min} [K] at 600 K PT inside the area where the equivalent latitude (EQL) is greater than 70°, corresponding to the area inside the Arctic polar vortex. The black solid line shows the mean value from 2001 to 2011. The red line is the T_{min} temporal evolution from 1 December 2009 to 31 March 2010. The shaded area encompasses the minimum/maximum T_{min} between 2001 and 2011.

ACPD
14, 7889–7916, 2014

Arctic ozone loss during 2009–2010 from Odin/SMR and SMILES

K. Sagi et al.

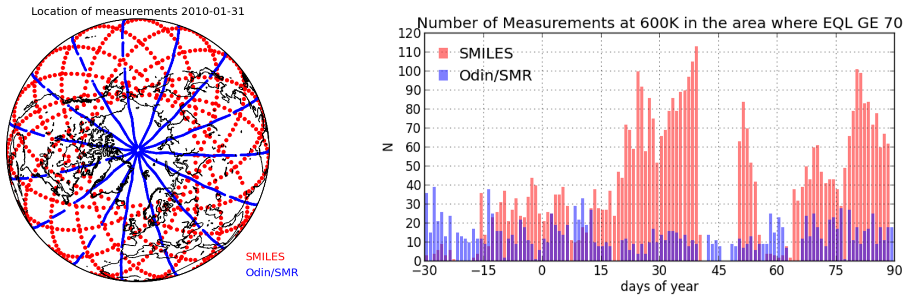

Fig. 2. (left) An example of the geographical distributions of O_3 observations from SMILES and Odin/SMR on 31 January 2010. (right) The number of measurements inside the area where the equivalent latitude is greater than 70° on a PT surface of 600 K. Note that measurements with measurement response below 0.85 are filtered out.

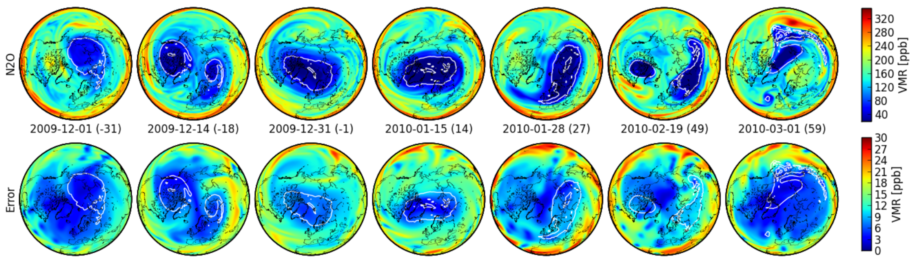

Fig. 3. Modeled N_2O fields with assimilation of SMR data (top) and their error fields (bottom) on selected dates at 600K level. The white contour lines indicate the vortex edge (EQL= 70°).

ACPD
14, 7889–7916, 2014

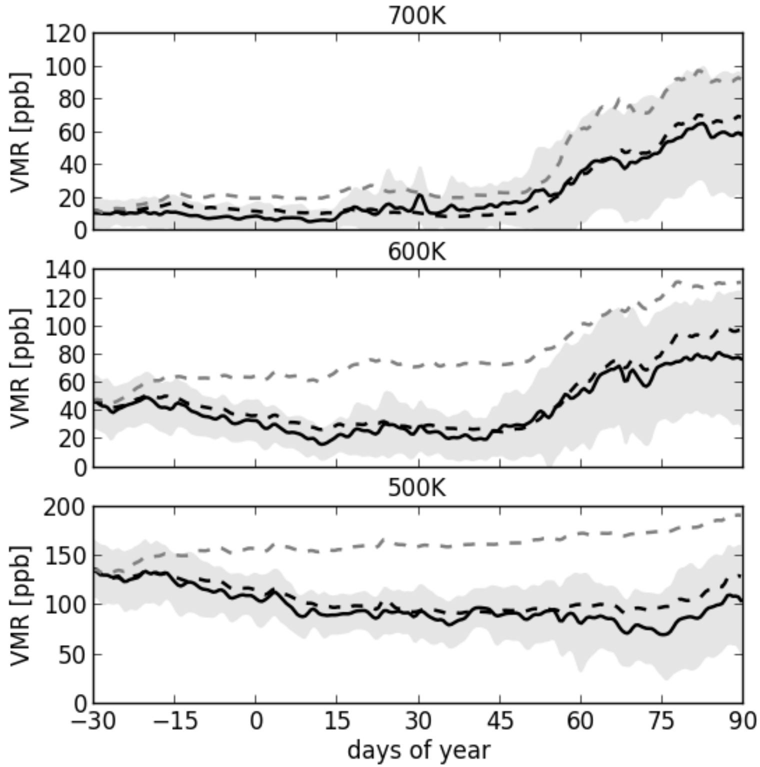

Fig. 4. Time series of the vortex mean N_2O mixing ratio in the DIAMOND model at selected PT levels. The solid line shows the average inside the area where the EQL is ≥ 70°, calculated from the assimilated field of Odin N_2O. The dashed lines show vortex means of predictions initiated on 1 December, using the 2D off-line advection model including vertical transport (black) and the advection model without any vertical transport (gray). The shaded area indicates the estimated error (more detail can be seen in Fig. 5).

ACPD
14, 7889–7916, 2014

Arctic ozone loss during 2009–2010 from Odin/SMR and SMILES

K. Sagi et al.

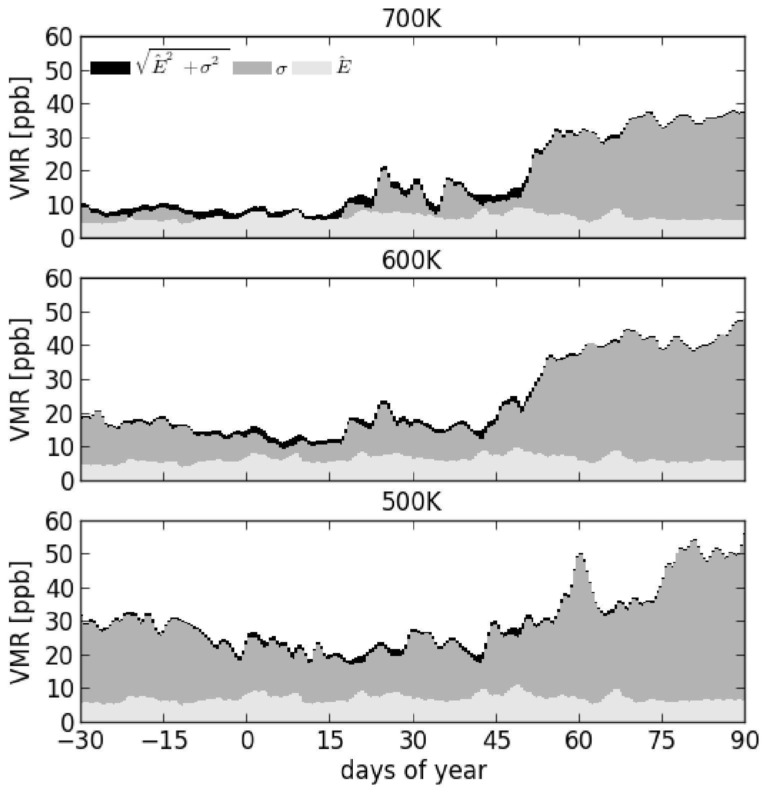

Fig. 5. The estimated uncertainty of the vortex mean of N_2O. The dark gray area shows the standard deviation (σ) inside the vortex (EQL $\geq$ 70). The light gray area shows the vortex mean of the error fields ($\hat{E}$). Finally, the black area indicates the total estimated error, which has been calculated as $\sqrt{\sigma^2+\hat{E}^2}$ and is shown as uncertainties in Fig. 4.

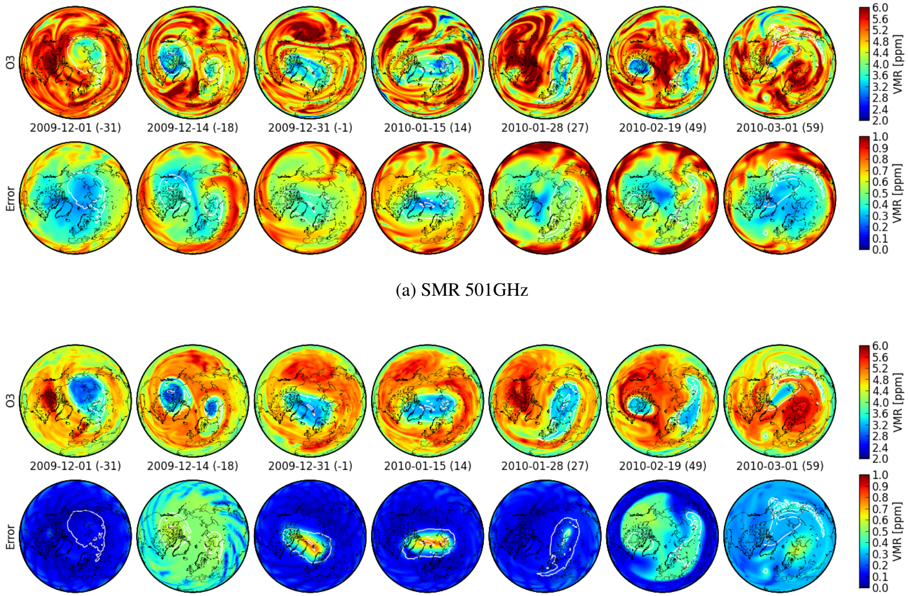

(a) SMR 501GHz

(b) SMILES

Fig. 6. Same as figure 3 but for O_3 from **(a)** SMR and **(b)** SMILES.

ACPD
14, 7889–7916, 2014

Arctic ozone loss during 2009–2010 from Odin/SMR and SMILES

K. Sagi et al.

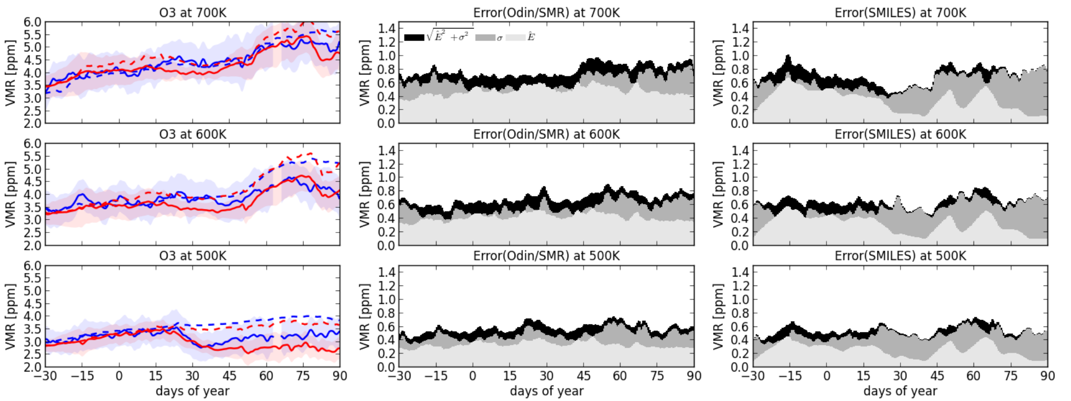

Fig. 7. (Left panels) Same as figure 4 but for O_3 from SMR (blue) and SMILES (red). (Middle panels) Same as figure 5 but for O_3 from SMR. (Right panels) Same as figure 5 but for O_3 from SMILES.

ACPD
14, 7889–7916, 2014

Arctic ozone loss during 2009–2010 from Odin/SMR and SMILES

K. Sagi et al.

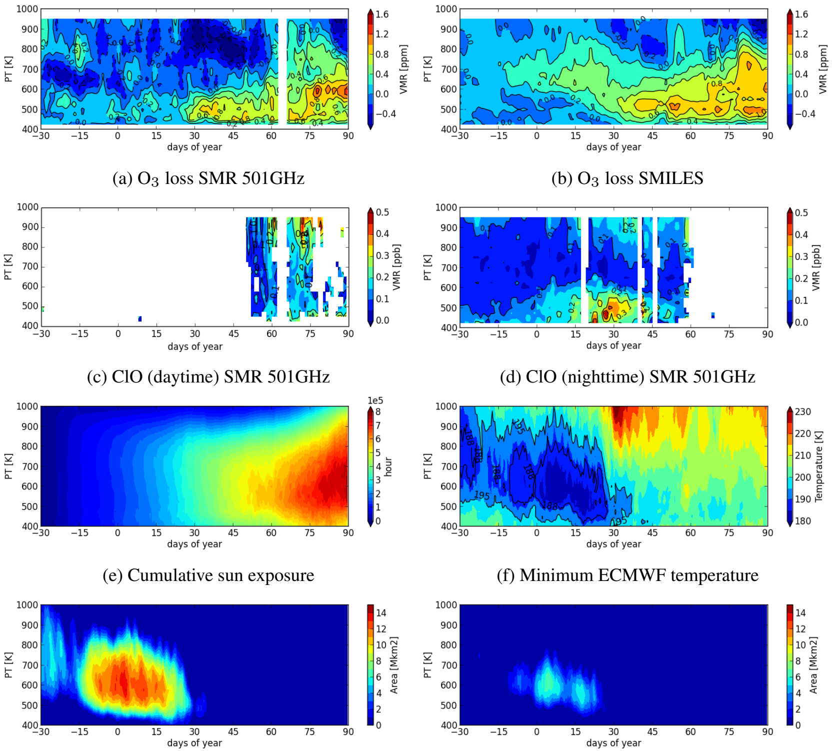

(a) O_3 loss SMR 501GHz
(b) O_3 loss SMILES
(c) ClO (daytime) SMR 501GHz
(d) ClO (nighttime) SMR 501GHz
(e) Cumulative sun exposure
(f) Minimum ECMWF temperature
(g) Area with temperatures below 195K
(h) Area with temperatures below 188K

Fig. 8. Several parameters as a function of time (days from 1 January 2010) and isentropic levels between 400K and 1000K. **(a, b)** Vortex mean O_3 loss derived from SMR and SMILES, respectively. **(c, d)** Vortex mean ClO retrieved from the SMR in daytime and nighttime, respectively. **(e)** Cumulative sun exposure time of the polar vortex. **(f)** Minimum air temperature inside the vortex derived from ECMWF. **(g, h)** Area where the temperature below T_{NAT} and T_{ice}, respectively.

ACPD
14, 7889–7916, 2014

K. Sagi et al.

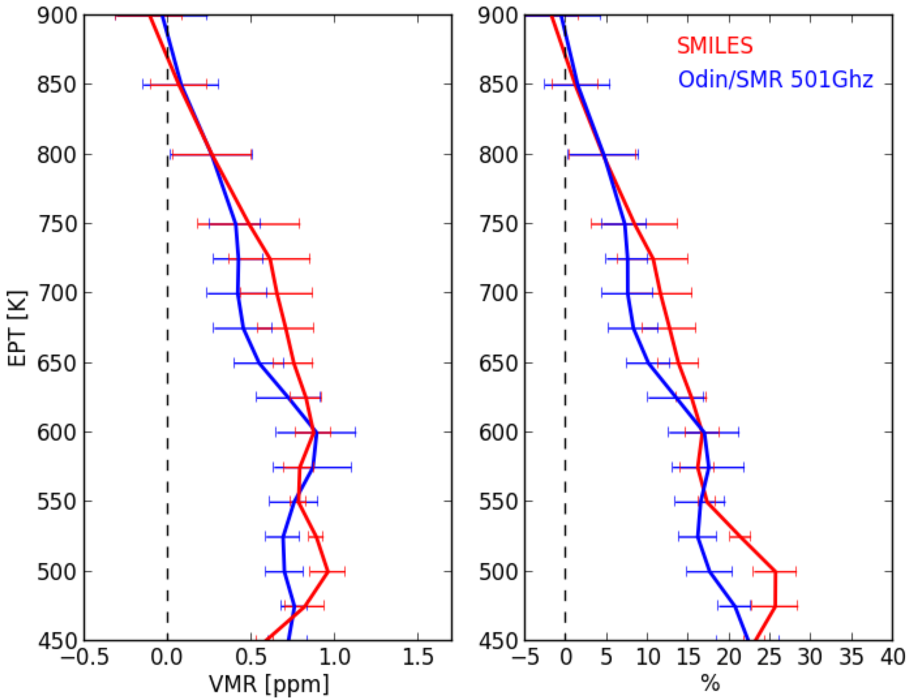

Fig. 9. Vertical profiles of monthly mean accumulated O_3 loss for March. Loss was derived by subtracting the passive ozone from the active ozone. The error bars are given as the standard deviation of derived daily O_3 loss inside the vortex for this period. The left panel shows loss in VMR, and the right panel shows relative losses in percent.

ACPD
14, 7889–7916, 2014

Arctic ozone loss during 2009–2010 from Odin/SMR and SMILES

K. Sagi et al.